Self-mediation of runaway electrons via self-excited wave-wave and wave-particle interactions

Qile Zhang, Yanzeng Zhang, and Xian-Zhu Tang
*Los Alamos National Laboratory, Los Alamos, NM 87545, USA**

Qi Tang
School of Computational Science and Engineering,
Georgia Institute of Technology, Atlanta, GA 30332, USA

Nonlinear dynamics of runaway electron induced wave instabilities can significantly modify the runaway distribution critical to tokamak operations. Here we present the first-ever fully kinetic simulations of runaway-driven instabilities towards nonlinear saturation in a warm plasma as in tokamak start up. It is found that the slow-X modes grow an order of magnitude faster than the whistler modes, and they parametrically decay to produce whistlers much faster than those directly driven by runaways. These parent-daughter waves, as well as secondary and tertiary wave instabilities, initiate a chain of wave-particle resonances that strongly diffuse runaways to the backward direction. This reduces almost half of the current carried by high-energy runaways, over a time scale orders of magnitude faster than experimental shot duration. These results beyond quasilinear analysis may impact anisotropic energetic electrons broadly in laboratory, space and astrophysics.

Introduction.— One of the most efficient ways to generate relativistic electrons in a dilute plasma is runaway acceleration by a strong electric field along the magnetic field, [1, 2] coupled with an avalanche growth mechanism due to knock-on collisions between primary runaways and background cold electrons [3–5]. Plasma wave instabilities excited by these relativistic runaway electrons [6–8] and their roles in modifying the runaway electron distribution through nonlinear wave-particle interaction, have piqued long-standing interest from both a basic plasma physics perspective and the practical need of mitigating runaway electrons in tokamak plasmas. The latter comes about because the runaways can cause severe damage on the plasma-facing components during both tokamak startup [9–11] and major disruptions [12–14], which presents a critical challenge for tokamak power reactors. [15, 16] Outside magnetic fusion, interaction of energetic electrons and their self-induced waves plays critical roles in regulating the transport and heat flux induced by these energetic electrons, for example, in Earth's magnetosphere [17], solar flares [18] and astrophysical intracluster medium [19]. To facilitate these and similar applications in a variety of laboratory, space, and astrophysical plasmas, we must understand the basic plasma physics of runaway-wave interaction and its nonlinear saturation.

Recent experimental advances in diagnosing the runaway electron distribution, via, for example, spatial, temporal, and energetically resolved measurement of bremsstrahlung hard-x-ray emission, provide information on the energy and pitch dependence of the runaway electron distribution. [20] Direct measurement of high-frequency electromagnetic waves in tokamak experiments supplied the evidence of runaway-induced plasma wave instabilities. [21] These hardware advances offer an unprecedented opportunity to contrast predictions from theory and simulations with experimental observations. [20–22] The most remarkable success to date has been on the role of forward-propagating (with respect to the runaway direction) whistler waves that are excited by runaways via the anomalous Doppler-shifted cyclotron resonances. [22–24] This finding can be contrasted with the physical picture that extraordinary waves above the whistler branch, also known as the slow-X modes [25], can be excited by the runaway electrons via the same resonance [26, 27]. Most intriguingly, these authors [26, 27] also found that being of much higher frequency than the whistler branch, the slow-X modes could have much higher growth rates and stronger quasilinear pitch angle diffusion, from an analysis using a model runaway distribution. The instrumentation limitation in previous DIII-D experiments [21] prevents direct measurement of the primary whistler modes, let alone the even higher frequency X-modes. This leaves these two distinct physical scenarios unresolved: one dominated by whistler instability and the other by slow-X modes.

Further complicating the situation, the saturation physics of these runaway wave instabilities were previously examined using the quasilinear theory, for both whistler and slow-X branches. [22, 26] Common concerns for quasilinear saturation analysis include (1) the mischaracterization of saturated states if nonlinear coupling is the dominant mechanism; (2) even for systems that saturate at the marginal stability boundary, inclusion of parametric decay instability and secondary/tertiary instability associated with an evolving distribution function, often neglected or incomplete, can be essential for accuracy but it is not known *a priori*; and (3) the quasilinear diffusion approximation can be problematic. First-principles nonlinear kinetic simulation is thus a necessary examination for physics fidelity and may guide the improvement of quasilinear analysis if it applies at all.

Here, for the first time, fully kinetic particle-in-cell simulations are successfully deployed to study runaway self-driven instabilities toward nonlinear saturation, initiated by a self-consistent runaway distribution from a drift-kinetic solver. We find that the slow-X modes grow an order of magnitude faster than the whistler modes, confirming an intriguing feature previously noted in Ref. [26, 27], and they go through parametric decay to produce whistlers much faster than those directly driven by runaways. More interestingly, the slow-X waves can initiate a chain of wave-particle resonances that strongly diffuse runaways to the opposite (backward) direction at moderate and high energy, which occurs much faster than the time scales of collisional current damping and runaway acceleration. These backward diffusion processes strongly modify the runaway distribution and reduce almost half of the runaway current. The new physics findings significantly modify what is known in the literature on runaway-wave dynamics mentioned above.

Numerical methods.— We deploy the typical tokamak start-up parameters $J = 2MA/m^2, n_e = 0.6 \times 10^{19} m^{-3}, T_e = 320eV, B = 1.45T$ with $\omega_{ce}/\omega_{pe} = 1.84$. From a relativistic drift-kinetic Fokker-Planck-Boltzmann (FPB) solver [28, 29], we compute the runaway electron distribution in the runaway avalanche regime with a strong electric field $E = 65E_c$ (with E_c the Connor-Hastie field [30]). Such an electric field is quite reasonable in a start up scenario [31]. The momentum space distribution of runaways has a low energy boundary at $p = 3m_e v_{te}$ that matches onto a bulk Maxwellian-Jüntter distribution with $v_{te} = \sqrt{2T_e/m_e}$ the electron thermal speed of the background plasma. When the runaway avalanche exponentially increases the runaway current to the total current, the resulting runaway distribution is fed into the fully kinetic VPIC code [32] to study the self-induced instabilities and wave-particle interactions on a much faster time scale compared to the small- and large-angle collisions, and radiation damping.

The VPIC simulations use proton-electron plasma with the realistic proton-electron mass ratio. The temperature $T_e = 320eV$ corresponds to a thermal-to-light speed ratio $v_{te}/c = 0.035$. The grid size is $\Delta_x = 0.0125 d_e = 0.5\lambda_{de}$, with $d_e = c/\omega_{pe}$ the electron inertial length and ω_{pe} the electron plasma frequency, and λ_{de} the electron Debye length. The time step is $dt\omega_{pe} = 0.01$. Considering the huge difference in particle number densities between the thermal and runaway electrons ($n_{re} = 0.0082 n_e$), we employ the weighted macro-particle approach for the thermal (with $p < 3m_e v_{te}$) and runaway (with $p > 3m_e v_{te}$) electrons. Specifically, we represent the runaway tail population with a 10 times smaller macro-particle weight compared to the thermal electrons so that the macro-particle number for runaways is enhanced by 10 times for better statistics. 2700 macro-particles per cell are used for the thermal electrons. As a simplified setup, the PIC simulation includes one spatial dimension with periodic boundary, three velocity dimensions, and an initially uniform magnetic field and plasma. This corresponds to the tokamak magnetic axis without the effect of trapped electrons. Since the distribution carries a parallel current $J = 2MA/m^2$, to be consistent with the uniform field, we Lorentz boost all electrons opposite to the runaway direction by the averaged parallel velocity $v_d = 0.007351c$ to cancel the current. Since $v_d \ll v_{te}$, the effect of this boost on the electron distribution is minimal. To make wave modes sufficiently continuous over k as in reality, we use a long enough periodic domain size $L_x = 1344 d_e$ to ensure a small wave mode spacing $\Delta k = 2\pi/L_x$. The spatial dimension is at an angle θ to the magnetic fields, which is chosen as $\theta = 40°$. Our linear dispersion analysis following Ref. [22, 23] shows that, for such $\theta = 40°$, the growth rate of slow-X modes ($\sim 4 \times 10^{-3}\omega_{pe}$) is an order of magnitude larger than that of the fastest whistler mode ($\sim 10^{-4}\omega_{pe}$), which is excited at $\theta \sim 70°$. We run the simulation till the distribution saturates, which is at $t\omega_{pe} \sim 10^6$. The collisional damping time scales [23] of the relevant waves ($t\omega_{pe} \sim 10^7 - 10^8$) are much longer than the whole simulation, so we can neglect collisions.

Strong slow-X mode drive and its parametric decay at short time scale.— Based on the dispersion analysis, the high-energy runaway tail ($p/m_e c \sim 30$) can drive waves through $n = -1$ anomalous Doppler resonance not only on the whistler branch [22, 33] but also on the slow-X branch [26, 27]. Here the resonance condition reads

$$\omega - k_{\parallel} V \xi = n\omega_{ce}/\gamma, \tag{1}$$

where $\omega_{ce} > 0$. For $\theta = 40°$, the maximum growth rate for the slow-X branch is $\sim 4 \times 10^{-3}\omega_{pe}$, much higher than the whistler branch $\sim 10^{-5}\omega_{pe}$. As shown in the Fourier space at very early time $t\omega_{pe} < 5000$ in Fig. 1, the amplitude of slow-X waves in the red box has grown large, with even nonlinearly generated higher harmonics that have multiples of ω and k [34].

Once the strongest forward propagating slow-X mode grows to a large amplitude, it can go through parametric decay to produce two pairs of lower frequency modes (e.g., see Fig. 1), including forward whistler waves. Specifically, the strongest slow-X wave (blue star, $\omega = 0.86\omega_{ce} = 1.58\omega_{pe}, kd_e = 2.16$) parametrically decays into two pairs of wave groups (red or green triangles). The red triangles include a low frequency whistler wave ($\omega \sim 0.07\omega_{ce} = 0.13\omega_{pe}, kd_e \sim 0.35$), and a high frequency slow-X wave ($\omega \sim 0.8\omega_{ce} = 1.47\omega_{pe}, kd_e \sim 1.88$) near the parent wave. The green triangles can also produce whistler waves at higher ω and k ($kd_e \sim 1 - 2$). These parametric decay processes are much faster than the whistler modes directly driven by the runaways, i.e. the primary whistler modes. These daughter whistlers observe high amplitude and broad spectrum.

We will explore the runaway dynamics in the momentum space over pitch ξ and momentum p. The diffusion

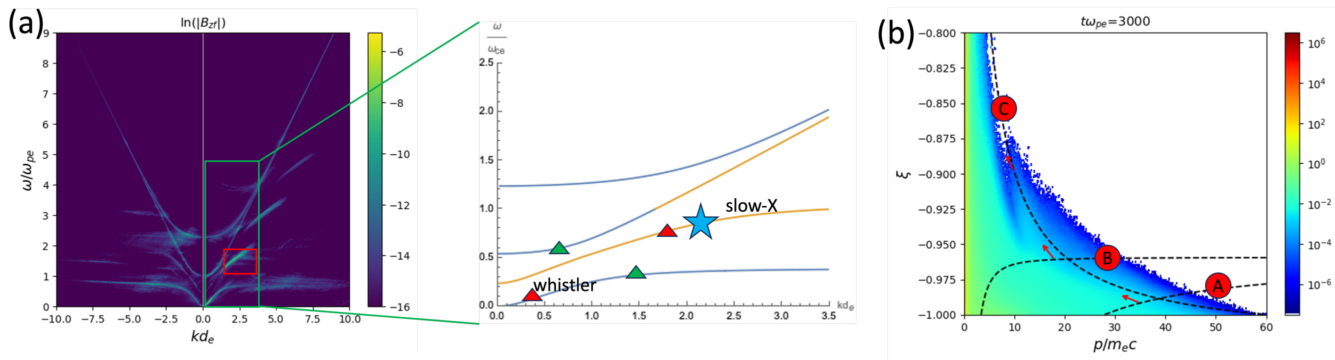

FIG. 1. (a): the Fourier space of magnetic field B_z where slow-X waves are strongly driven (red box). A schematic picture of a zoom-in window (green box) on the Fourier space from cold plasma dispersion [35] illustrates different branches (especially the whistler and slow-X), and different waves on the branches. The strongly driven parent slow-X mode (blue star) can parametrically decay into two pairs of daughter wave groups (red or green triangles), both including whistler waves. (b): in the momentum space distribution, the slow-X waves diffuse the high-energy tail over pitch and momentum at this early time, as shown by the resonance lines (dashed lines) and diffusion directions (red arrows).

direction of runaway electrons in the local momentum space by an individual resonant wave (satisfying Eq. (1)) can originate from the directional gradient of the runaway distribution $f(p, \xi)$ as $\hat{L}f$, where

$$\begin{aligned}\hat{L} &= \frac{1}{p}\frac{\partial}{\partial p} - \frac{1}{p^2}\frac{n\omega_{ce}/\gamma - \omega(1-\xi^2)}{\omega\xi}\frac{\partial}{\partial \xi} \\ &= -(-\frac{1}{p}, \frac{1}{p^2}(\xi - k_\parallel v/\omega)) \cdot (\frac{\partial}{\partial p}, \frac{\partial}{\partial \xi}).\end{aligned} \tag{2}$$

Since the wave is driven by the gradient $\hat{L}f$ and the quasi-linear diffusion of f is given by $\hat{L}^2 f$ [22, 35], the diffusion direction can be defined by the unit vector

$$\hat{\mathbf{g}} = (-\frac{1}{p}, \frac{1}{p^2}(\xi - k_\parallel v/\omega))/\|(-\frac{1}{p}, \frac{1}{p^2}(\xi - k_\parallel v/\omega))\| * sgn(\hat{L}f) \tag{3}$$

This vector in fact represents the particle flux direction when the wave is smoothing out the gradient $\hat{L}f$. It must be noted that the runaway electrons can either lose (diffused towards small p, positive $\hat{L}f$) energy to or gain (towards large p, negative $\hat{L}f$) from the resonant wave. The former corresponds to runaways driving the wave. The latter will cause the wave damping by the runaways, in which case the wave must be driven by other mechanisms (e.g., the parametric decay) or by different resonances. We will use two arrow colors (red and blue) to denote the wave gaining/losing energy from the wave-particle interaction in the local momentum space.

During the short time scale $t\omega_{pe} < 5000$, the slow-X modes, including the parent and daughter waves, can notably diffuse the high energy runaway tail ($p > 10m_e c$), which initiates the fast backward diffusion. Fig. 1(b) shows zoom-in high energy runaway tail distribution close to $\xi = -1$. The high-energy electrons are being diffused subsequently along diffusion directions on different resonance lines. Specifically, from resonance lines A to C, they involve resonances $n = -1$ and $n = 0$ of the parent slow-X wave ($\omega = 1.58\omega_{pe}, kd_e = 2.16$), and $n = 1$ of the daughter slow-X wave ($\omega = 1.47\omega_{pe}, kd_e = 1.88$). They lead to a finger in $f(p, \xi)$ towards lower energy and higher pitch, which drives primary and secondary slow-x modes. Meanwhile, these strong parent and daughter slow-X modes also accelerate electrons, from the edge of the backward thermal bulk, along the resonance line of $n = 1$ to higher energy as shown in Fig. 2(a) (label A for mode $\omega = 1.53\omega_{pe}, kd_e = 2$). This establishes a strong finger in $f(p, \xi)$, by damping all the slow-X waves. Notice that this extended finger will contribute to the forward current at moderate energy.

Fast backward diffusion at moderate energy at medium time scale.— During the medium time scale ($tw_{pe} \sim 3 \times 10^4$), the strong finger from the damping of slow-X modes can initiate a chain of wave-particle interactions through $n = 1$ resonance, which can diffuse moderate energy runaways ($p/m_e c \sim 5$) to the backward direction (e.g., see Fig. 2(b)). The strong finger first provides free energy to trigger a series of secondary backward propagating whistler waves (visible in the Fourier space in Fig. 1(a)) through $n = 1$ resonance (e.g., the red arrow at resonance line B for $\omega = 0.2\omega_{pe}, kd_e = 0.47$). These secondary whistlers can further diffuse the runaways towards higher pitch (the blue arrow on B), forming another finger. This new finger sequentially encounters the resonance lines of $n = 1$ of the forward whistler waves from the parametric decay of slow-X such as: label C ($\omega = 0.28\omega_{pe}, kd_e = 0.61$) and label D ($\omega = 0.18\omega_{pe}, kd_e = 0.45$), which diffuse runaway electrons straight to the backward direction.

Fast backward diffusion at high energy at long time scale.— Following the fast backward diffusion of high-energy runaways by the slow-X modes, the whistler waves produced from the parametric decay process of the

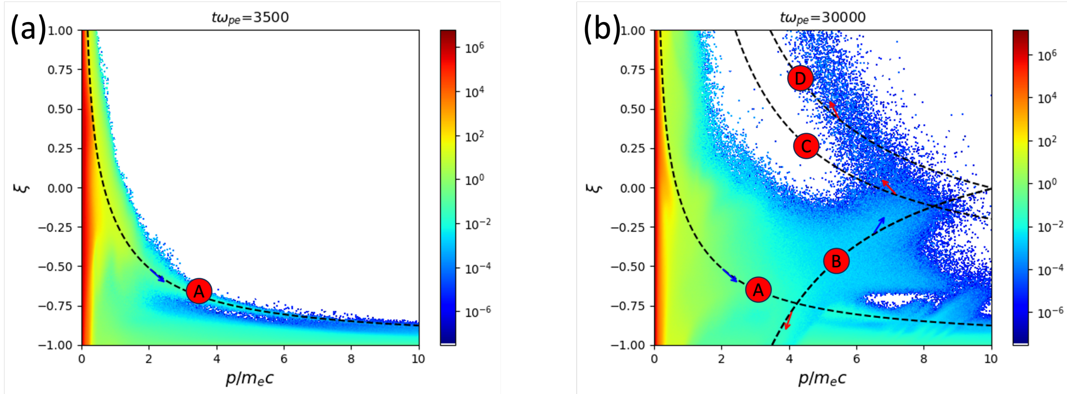

FIG. 2. The momentum space at moderate energy at different times. The strong slow-x waves initiate a chain of wave-particle resonances labeled as ABCD that diffuse runaways to the backward direction along their diffusion directions.

slow-X mode can continue to backward diffuse the high-energy runaway tail through a chain of resonances over a long time scale $tw_{pe} \sim 3 \times 10^5$, as shown in Fig. 3. Specifically, Fig. 3(a) shows the backward diffusion of runaways on different resonance lines of an example forward whistler wave $\omega = 0.13\omega_{pe}, kd_e = 0.35$ near the peak of the whistler spectrum from the parametric decay, sequentially with $n = -2$ to 2 resonances from label A to E. This forms a strong diffusion finger straight to backward. The quasi-linear diffusion [35, 36] of these different harmonic resonances can be connected to each other by the broad spectrum of whistler waves from parametric decay (see diffusion coefficients in the supplemental material). The backward diffusion to lower energy also allows the excitation of secondary whistler waves, which further enhance the diffusion at later time.

The distinct backward finger formed at high energy introduces free energy to trigger a series of tertiary backward whistler waves through $n = 1, 2$ resonances. An example resonance line of $n = 2$ in Fig. 3(b) (label A) is shown for a backward whistler mode $\omega = 0.09\omega_{pe}, kd_e = 0.28$, which is driven by the high-energy runaways at $p/m_ec \sim 22$ and $\xi \sim -0.35$ (the red arrow). Once it is excited, it will diffuse electrons of $p/m_ec \sim 14$ (the blue arrow) to higher pitch to encounter the broad spectra of resonance lines of $n = 0, 1, 2$ (label B to D) of the forward whistler waves (e.g. $\omega = 0.15\omega_{pe}, kd_e = 0.38$). Eventually, the high-pitch momentum space at high energy ($p/m_ec \geq 10$) is significantly filled. See also the supplemental movie demonstrating all the fast backward diffusion processes. Fig. 3(c) shows the evolution of the integrated current distribution over momentum during this process. We have reversed the previous Lorentz boost of v_d to retrieve the current before the integration. The current contained at the high-energy runaway tail decreases significantly over time as the average pitch of high-energy electrons increases. When the current profile eventually saturates, almost half of the high energy current (e.g. $p/m_ec > 10$, above 5MeV) is converted to be carried by lower energy superthermal electrons at $p/m_ec \lesssim 1$. This whole strong process occurs at a fast time scale of $3 \times 10^5 w_{pe}^{-1} \sim 10^{-6}s$, which is extremely short compared to experimental shot duration or the collisional runaway current damping time scale $\tau_c = 4\pi\epsilon_0^2 m_e^2 c^3/e^4 n_e ln\Lambda \sim 0.37s$, with $ln\Lambda$ the Coulomb Logarithm. Note that the superthermal current at $0.3 < p/m_ec \lesssim 1$ significantly increases over time, contributed by multiple processes. While the early time superthermal current is significantly contributed by the strong finger extending to moderate energy from the $n = 1$ damping of slow-X waves, at the later time it is contributed by both $n = 0$ landau damping of the forward whistlers and $n = 1$ damping of the backward whistlers. Interestingly, this increasing superthermal current results in parallel electric fields that push the thermal bulk backward due to current conservation (Ampere's law), leading to negative integrated current from the bulk electrons with $p/m_ec < 0.2$.

Discussion.— First fully kinetic simulations of the excitation and nonlinear saturation of runaway-electron-driven electromagnetic wave instabilities reveals a qualitatively new physics picture of complex wave-wave interactions and runaway-wave-interaction-induced secondary and tertiary wave instabilities, in contrast to previous quasilinear analysis emphasizing only the primary instability. The slow-X modes, found to be the fastest growing instabilities, can parametrically drive both high and low frequency whistlers, often dominating over the primary whistler modes that are directly driven by the runaways. Wave-particle resonant interaction develops rapidly evolving features in momentum space for the electron distribution function, including particle acceleration, slowing down, and strong pitch diffusion. The secondary and tertiary wave instabilities are sequentially excited to facilitate rapid pitch spread to backward for runaways and the growth of superthermal electrons, with the net result of quickly transferring substantial plasma current from high-energy runaways to medium-energy

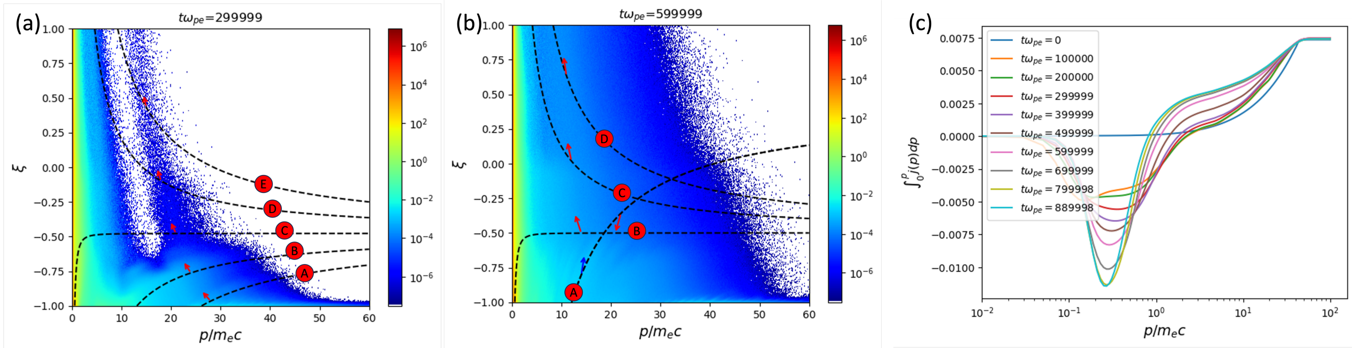

FIG. 3. (a): in the high-energy momentum space, the backward diffusion occurs sequentially along the diffusion directions of multiple resonances of forward whistler waves. (b) at later time the triggered backward whistlers diffuse electrons to higher pitch to encounter resonances of forward whistlers. Eventually the backward diffusion significantly fills the high pitch momentum space at high energy. (c): the integrated current distribution over momentum, where almost half of the integrated current at high energy is converted to lower energy during this process.

runaways and superthermal electrons, which is a form of runaway mitigation that limits the runaway energy and increases its dissipation.

As notable experimental signatures, one can expect both forward and backward [37] electromagnetic waves at large amplitudes, particularly the whistler branch, as well as strong chirping. Similarly, a large population of relativistic electrons can be measured to move in the opposite direction of the original distribution, i.e. in the co-current direction. Although the current simulations do not account for magnetic trapping, the same wave-runaway interaction physics should lead to a significant trapped high-energy electron population through wave-induced pitch angle scattering. This can provide a robust drive for Alfvén waves in the MHz range that were observed in experiments and thought to be driven by processional drift resonance with trapped runaways [38–40].

While we initialize the kinetic simulations with the slow-time-scale FPB solution to explore these fast-time-scale wave dynamics, how the wave instabilities and distributions self-consistently couple on a slow time scale remains to be further explored. The physical effects of tokamak geometry such as trapped electrons, spatial dependence and radial transport need to be explored with simulations of higher dimensions. The revealed basic processes of fast backward diffusion facilitated by the slow-X waves may impact not only the runaway electron dynamics in tokamaks, but also likely the anisotropic energetic electron evolution and transport broadly in space and astrophysics [17–19].

SUPPLEMENTAL MATERIAL

See Fig. S1 for the quasi-linear diffusion coefficient $D_{\xi\xi}$ at two different times showing the different harmonic resonances connected to each other by the broad spectrum of whistler waves. The excitation of secondary whistler waves by the backward diffusion further enhances the diffusion coefficient at the later time.

Acknowledgment We thank the U.S. Department of Energy Office of Fusion Energy Sciences and Office of Advanced Scientific Computing Research for support under the Tokamak Disruption Simulation and SCREAM Scientific Discovery through Advanced Computing (SciDAC) project, the Base Fusion Theory Program, and more recently the General Plasma Science program, all at Los Alamos National Laboratory (LANL) under contract No. 89233218CNA000001. This research used resources of the National Energy Research Scientific Computing Center, a DOE Office of Science User Facility supported by the Office of Science of the U.S. Department of Energy under Contract No. DE-AC02-05CH11231 using NERSC award FES-ERCAP0028155 and the Los Alamos National Laboratory Institutional Computing Program, which is supported by the U.S. Department of Energy National Nuclear Security Administration under Contract No. 89233218CNA000001.

* qlzhang@lanl.gov

[1] H. Dreicer, Electron and ion runaway in a fully ionized gas. i, Phys. Rev. **115**, 238 (1959).

[2] J. Connor and R. Hastie, Relativistic limitations on runaway electrons, Nuclear Fusion **15**, 415 (1975).

[3] I. SOKOLOV, Multiplication' of accelerated electrons in a tokamak, JETP Letters **29**, 218 (1979).

[4] R. Jayakumar, H. Fleischmann, and S. Zweben, Collisional avalanche exponentiation of runaway electrons in electrified plasmas, Physics Letters A **172**, 447 (1993).

[5] M. Rosenbluth and S. Putvinski, Theory for avalanche of runaway electrons in tokamaks, Nuclear Fusion **37**, 1355 (1997).

[6] V. Parail and O. Pogutse, The kinetic theory of runaway electron beam instability in a tokamak, Nuclear Fusion **18**, 303 (1978).

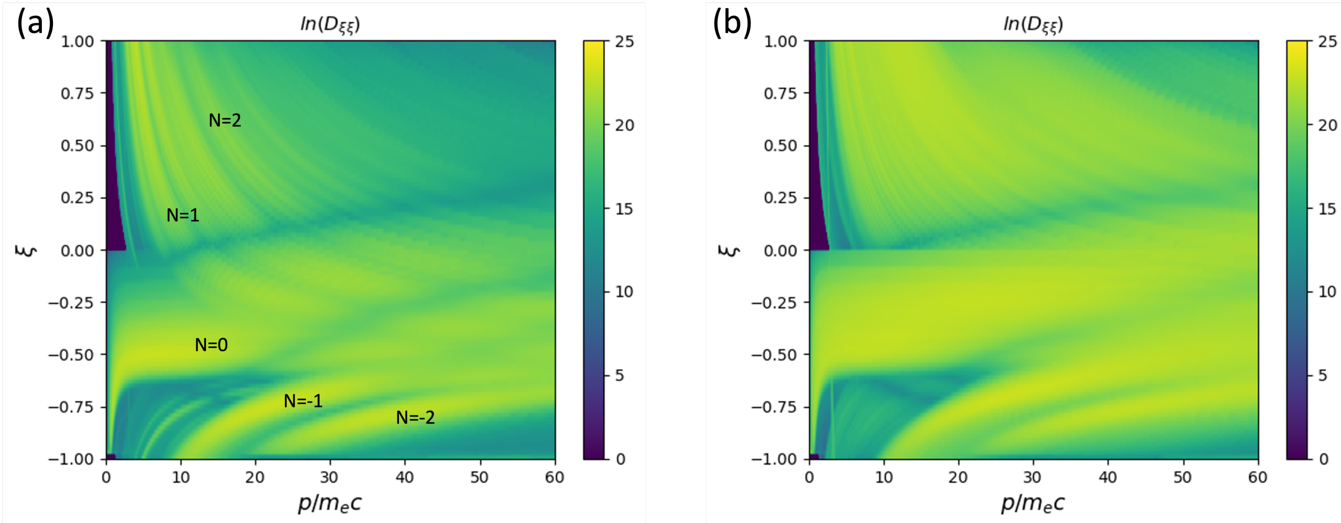

FIG. S1. Quasilinear diffusion coefficient $D_{\xi\xi}$ (arbitrary unit) in the momentum space calculated from the forward whistler branch ($kd_e \in [0, 2]$) in the Fourier space, involving n=-2 to 2 resonances for (a) $t\omega_{pe} = 5000$ and (b) $t\omega_{pe} = 250000$.

[7] G. I. Pokol, A. Kómár, A. Budai, A. Stahl, and T. Fülöp, Quasi-linear analysis of the extraordinary electron wave destabilized by runaway electrons, Physics of Plasmas **21**, 102503 (2014), _eprint: https://pubs.aip.org/aip/pop/article-pdf/doi/10.1063/1.4895513/14862963/102503_1_online.pdf.

[8] P. Aleynikov and B. Breizman, Stability analysis of runaway-driven waves in a tokamak, Nuclear Fusion **55**, 043014 (2015).

[9] P. de Vries and Y. Gribov, Iter breakdown and plasma initiation revisited, Nuclear Fusion **59**, 096043 (2019).

[10] P. C. de Vries, Y. Gribov, R. Martin-Solis, A. B. Mineev, J. Sinha, A. C. C. Sips, V. Kiptily, A. Loarte, and contributors JET, Analysis of runaway electron discharge formation during joint european torus plasma start-up, Plasma Physics and Controlled Fusion **62**, 125014 (2020).

[11] M. Hoppe, I. Ekmark, E. Berger, and T. Fülöp, Runaway electron generation during tokamak start-up, Journal of Plasma Physics **88**, 905880317 (2022).

[12] T. Hender, J. Wesley, J. Bialek, A. Bondeson, A. Boozer, R. Buttery, A. Garofalo, T. Goodman, R. Granetz, Y. Gribov, *et al.*, Mhd stability, operational limits and disruptions, Nuclear fusion **47**, S128 (2007).

[13] A. H. Boozer, Theory of runaway electrons in iter: Equations, important parameters, and implications for mitigation, Physics of Plasmas **22**, 032504 (2015).

[14] B. N. Breizman, P. Aleynikov, E. M. Hollmann, and M. Lehnen, Physics of runaway electrons in tokamaks, Nuclear Fusion **59**, 083001 (2019).

[15] N. W. Eidietis, Prospects for disruption handling in a tokamak-based fusion reactor, Fusion Science and Technology **77**, 738 (2021), https://doi.org/10.1080/15361055.2021.1889919.

[16] A. J. Creely, D. Brunner, R. T. Mumgaard, M. L. Reinke, M. Segal, B. N. Sorbom, and M. J. Greenwald, SPARC as a platform to advance tokamak science, Physics of Plasmas **30**, 090601 (2023), _eprint: https://pubs.aip.org/aip/pop/article-pdf/doi/10.1063/5.0162457/19982805/090601_1_5.0162457.pdf.

[17] J. Yu, J. Wang, Z. He, Z. Chen, L. Li, J. Cui, and J. Cao, Electron diffusion by chorus waves: effects of latitude-dependent wave power spectrum, Frontiers in Astronomy and Space Sciences **10**, 10.3389/fspas.2023.1333184 (2023).

[18] G. T. Roberg-Clark, O. Agapitov, J. F. Drake, and M. Swisdak, Scattering of Energetic Electrons by Heat-flux-driven Whistlers in Flares, ApJ **887**, 190 (2019), arXiv:1908.06481 [physics.space-ph].

[19] G. T. Roberg-Clark, J. F. Drake, C. S. Reynolds, and M. Swisdak, Suppression of Electron Thermal Conduction by Whistler Turbulence in a Sustained Thermal Gradient, Phys. Rev. Lett. **120**, 035101 (2018), arXiv:1709.00057 [astro-ph.HE].

[20] C. Paz-Soldan, C. M. Cooper, P. Aleynikov, D. C. Pace, N. W. Eidietis, D. P. Brennan, R. S. Granetz, E. M. Hollmann, C. Liu, A. Lvovskiy, R. A. Moyer, and D. Shiraki, Spatiotemporal evolution of runaway electron momentum distributions in tokamaks, Phys. Rev. Lett. **118**, 255002 (2017).

[21] D. A. Spong, W. W. Heidbrink, C. Paz-Soldan, X. D. Du, K. E. Thome, M. A. Van Zeeland, C. Collins, A. Lvovskiy, R. A. Moyer, M. E. Austin, D. P. Brennan, C. Liu, E. F. Jaeger, and C. Lau, First direct observation of runaway-electron-driven whistler waves in tokamaks, Phys. Rev. Lett. **120**, 155002 (2018).

[22] C. Liu, E. Hirvijoki, G.-Y. Fu, D. P. Brennan, A. Bhattacharjee, and C. Paz-Soldan, Role of kinetic instability in runaway-electron avalanches and elevated critical electric fields, Phys. Rev. Lett. **120**, 265001 (2018).

[23] P. Aleynikov and B. Breizman, Stability analysis of runaway-driven waves in a tokamak, Nuclear Fusion **55**, 043014 (2015).

[24] B. N. Breizman and D. I. Kiramov, Marginal stability constraint on runaway electron distribution, Physics of Plasmas **30**, 022301 (2023), https://pubs.aip.org/aip/pop/article-pdf/doi/10.1063/5.0130558/19821968/022301_1_online.pdf.

[25] A. K. Ram and S. D. Schultz, Excitation,

propagation, and damping of electron Bernstein waves in tokamaks, Physics of Plasmas **7**, 4084 (2000), https://pubs.aip.org/aip/pop/article-pdf/7/10/4084/19087998/4084_1_online.pdf.

[26] G. I. Pokol, A. Kómár, A. Budai, A. Stahl, and T. Fülöp, Quasi-linear analysis of the extraordinary electron wave destabilized by runaway electrons, Physics of Plasmas **21**, 102503 (2014), arXiv:1407.5788 [physics.plasm-ph].

[27] A. Kómár, G. I. Pokol, and T. Fülöp, Interaction of electromagnetic waves and suprathermal electrons in the near-critical electric field limit, in *Journal of Physics Conference Series*, Journal of Physics Conference Series, Vol. 401 (2012) p. 012012.

[28] Z. Guo, C. J. McDevitt, and X.-Z. Tang, Phase-space dynamics of runaway electrons in magnetic fields, Plasma Physics and Controlled Fusion **59**, 044003 (2017).

[29] Z. Guo, C. Mcdevitt, and X. Tang, Toroidal effect on runaway vortex and avalanche growth rate, Physics of Plasmas **26**, 082503 (2019), https://doi.org/10.1063/1.5055874.

[30] J. Connor and R. Hastie, Relativistic limitations on runaway electrons, Nuclear Fusion **15**, 415 (1975).

[31] P. C. de Vries, Y. Lee, Y. Gribov, A. B. Mineev, Y. S. Na, R. Granetz, B. Stein-Lubrano, C. Reux, P. Moreau, V. Kiptily, B. Esposito, D. J. Battaglia, J. R. Martin-Solis, and ITPA IOS Collaborators, Cross-machine comparison of runaway electron generation during tokamak start-up for extrapolation to ITER, Nuclear Fusion **63**, 086016 (2023).

[32] K. J. Bowers, B. J. Albright, L. Yin, B. Bergen, and T. J. T. Kwan, Ultrahigh Performance Three-dimensional Electromagnetic Relativistic Kinetic Plasma Simulation), Phys. Plasmas **15**, 055703 (2008).

[33] T. Fülöp, G. Pokol, P. Helander, and M. Lisak, Destabilization of magnetosonic-whistler waves by a relativistic runaway beam, Physics of Plasmas **13**, 062506 (2006), https://pubs.aip.org/aip/pop/article-pdf/doi/10.1063/1.2208327/13594424/062506_1_online.pdf.

[34] B. Shivamoggi, *Introduction to Nonlinear Fluid-Plasma Waves*, Mechanics of Fluids and Transport Processes (Springer Netherlands, 2012).

[35] T. Stix, *Waves in Plasmas* (American Inst. of Physics, 1992).

[36] Z. Guo, C. J. McDevitt, and X.-Z. Tang, Control of runaway electron energy using externally injected whistler waves, Physics of Plasmas **25**, 032504 (2018), https://pubs.aip.org/aip/pop/article-pdf/doi/10.1063/1.5019381/16154805/032504_1_online.pdf.

[37] F. Almagri, N. C. Hurst, C. B. Fores, *et al.*, private communication (2024).

[38] A. Lvovskiy, C. Paz-Soldan, N. W. Eidietis, A. D. Molin, X. D. Du, L. Giacomelli, J. L. Herfindal, E. M. Hollmann, L. Martinelli, R. A. Moyer, M. Nocente, D. Rigamonti, D. Shiraki, M. Tardocchi, and K. E. Thome, The role of kinetic instabilities in formation of the runaway electron current after argon injection in diii-d, Plasma Physics and Controlled Fusion **60**, 124003 (2018).

[39] A. Lvovskiy, W. Heidbrink, C. Paz-Soldan, D. Spong, A. D. Molin, N. Eidietis, M. Nocente, D. Shiraki, and K. Thome, Observation of rapid frequency chirping instabilities driven by runaway electrons in a tokamak, Nuclear Fusion **59**, 124004 (2019).

[40] C. Liu, A. Lvovskiy, C. Paz-Soldan, S. C. Jardin, and A. Bhattacharjee, Self-Consistent Simulation of the Excitation of Compressional Alfvén Eigenmodes and Runaway Electron Diffusion in Tokamak Disruptions, Phys. Rev. Lett. **131**, 085102 (2023), arXiv:2303.03622 [physics.plasm-ph].